An Absolute Falling Tube Viscometer

Fulin Gui
Mainstream Engineering Corporation,
Rockledge, Florida

Thomas F. Irvine, Jr.
Mechanical Engineering Department,
State University of New York,
Stony Brook, New York

■ A structurally simple absolute viscometer, the falling tube viscometer, with a large measurement range for viscosity from 0.5 to 10^9 cP (5×10^{-4} to 10^6 N s/m^2), has been extensively investigated. The flow field, shear rate, and pressure distribution in the viscometer have been obtained numerically to determine the entrance and exit effects. The viscometer was characterized by two variables, the geometry number Ge and the end correction factor. The former is exclusively determined by the dimensionless tube diameters and length and reflects the ratio of tube driving force to resistance. The latter is defined as the ratio of the actual to ideal geometry numbers. The results presented allow the prediction of end effects and geometry number without resorting to empirical corrections or instrument calibration. The agreement between the analytical and experimental results on the geometry number, the measured viscosity of standard fluids, repeatability, and accuracy is well within 1% in all cases. A correlation equation from which the geometry number can be calculated is presented that can be used to design viscometers for particular applications. Both the theoretical analysis and the experimental data indicate that falling tube viscometers based on the correlated equation are absolute viscometers with an accuracy within ±1.0%.

Keywords: *viscometer, falling tube viscometer, viscosity*

INTRODUCTION

The falling tube viscometer (FTV) was developed from the falling cylinder viscometer (FCV) [1,2], an asymptotic case of the FTV with a zero tube internal diameter. Figure 1 shows a schematic of the FTV consisting of a tube with flat ends and a cylindrical container, called the system, with the fluid to be measured. The tube falls vertically in the fluid along the axis of the system. With an appropriate instrument theory, the fluid viscosity can be measured from the terminal velocity of the falling tube if fluid and tube densities, gravitational acceleration, and tube and system geometries are known. The FTV has advantages over the FCV. The FTV has two shear surfaces and two flow channels inside and outside the tube providing flexibility to measure various ranges of viscosities, often low viscosities. In the case of moderate tube diameters, the two surfaces of the tube result in a large shear resistance that allows the FTV to be operated at the required low Reynolds number, including low-viscosity fluids. Within a certain viscosity range, the inside and outside diameters of the tube can be optimized to minimize any systematic errors due to tube construction and dimension measurement errors, thereby making the FTV more accurate than the FCV.

Previous applications of the instrument suffered from the disadvantage that the exact effect of the flow around the tube ends was unknown. Thus, the end shear and pressure forces could not be evaluated. With the emergence of computational methods, the flow field around the tube ends can now be clarified with the result that the FTV becomes an absolute instrument.

While the FCV [3–20] and its modification, the falling needle viscometer [21–26], have been frequently investigated, little was previously known about the FTV, especially its end effects. In 1971 Irving and Barlow [27], assuming a one-dimensional flow and neglecting the end effects, derived the relationship between the viscosity and the tube falling velocity as a function of three diameters instead of two dimensionless diameters. They predicted an error of 13%. Not knowing it was an FTV, McLachlan [28] used an "FCV" as a calibrated viscometer to measure the viscosity of polyphenol ether. The error he expected was 5%.

In this study, the FTV performance was investigated through an operational variable, the *geometry number* Ge, defined to characterize the FTV. It was first analyzed in the ideal case (an infinitely long tube) for a variety of combinations of tube diameters. Then computational results were obtained for the velocity, shear rate, and pressure distributions around the tubes for actual cases. The geometry numbers were thereafter evaluated numerically. An *end correction factor* (ECF), defined as the ratio of the

Address correspondence to Professor Thomas F. Irvine, Jr., Department of Mechanical Engineering, State University of New York at Stony Brook, Stony Brook, NY 11794-2300.
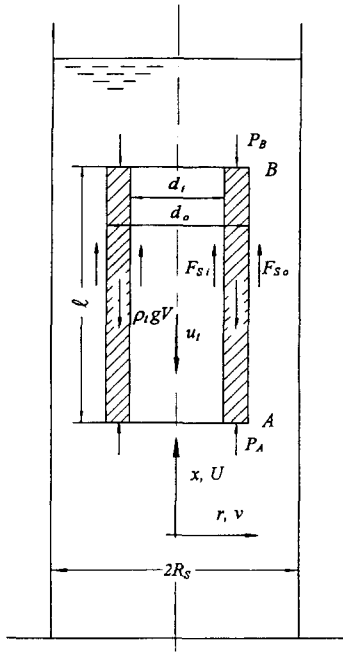
Figure 1. Schemetic of falling tube viscometer and coordinate system.

actual to the ideal geometry numbers and dominating the accuracy of the FTV, was examined extensively. A correlated equation for the ECF was extracted from a set of numerically computed and experimentally verified geometry numbers for the design and evaluation of viscometers. Experiments were conducted to determine the feasibility, reproducibility, and accuracy of the FTV. The agreement between the theoretical and experimental results indicates that a properly designed FTV can be an absolute instrument with an accuracy of $\pm 1.0\%$.

ANALYSIS

The Ideal Model

The ideal model is essentially an infinitely long tube with no end effects. The advantage of the ideal model is that the flow is one-dimensional and an analytical solution can be obtained. This solution can serve as a reference for the actual model. Using the coordinate system illustrated in Fig. 1, the dimensionless momentum equation for the flow around the tube is

$$\frac{1}{r^+}\frac{d}{dr^+}\left(r^+\frac{dU^+}{dr^+}\right) = -\frac{\mathrm{Re}_{R_s}}{2}\frac{dp^+}{dx^+}$$

$$= -\frac{f\mathrm{Re}_{R_s}}{2},$$

$$0 \le r^+ \le k_1 \text{ and } k_2 \le r^+ \le 1.0, \quad (1)$$

with boundary conditions

$$U^+(k_1) = -1.0, \qquad \frac{\partial U^+}{\partial r^+}(0) = 0,$$

$$U^+(k_2) = -1.0, \qquad U^+(1.0) = 0.$$

Accounting for the fluid displaced by the tube forward end, the continuity equation can be written as

$$\int_0^{k_1}U^+r^+\,dr^+ + \int_{k_2}^{1.0}U^+r^+\,dr^+ = \frac{k_2^2 - k_1^2}{2}. \quad (2)$$

When the tube reaches its terminal velocity, the driving force, which is equal to the difference between the gravitational and buoyancy forces, is balanced by the pressure on the tube ends and the shear forces on the sides. A force balance on the tube yields

$$\frac{(\rho_t - \rho_f)gR_s^2}{\mu u_t} = \frac{f}{2}\mathrm{Re}_{R_s} + \frac{2}{k_2^2 - k_1^2}$$

$$\times\left\{k_1\left|\left(\frac{dU^+}{dr^+}\right)_{k_1}\right| + k_2\left(\frac{dU^+}{dr^+}\right)_{k_2}\right\}. \quad (3a)$$

Solving Eqs. (1) and (2) by direct integration and evaluating the terms in Eq.(3a) yields

$$\frac{(\rho_t - \rho_f)gR_s^2}{\mu u_t}$$

$$= \mathrm{Ge}_i$$

$$= \frac{-2(1 + k_1^4 - k_2^4)}{(k_2^2 - k_1^2)\left[(1 - k_2^2)^2 + \ln k_2(1 + k_1^4 - k_2^4)\right]}, \quad (4a)$$

where Ge_i is called the ideal geometry number and is solely determined by the geometry of the viscometer, i.e., k_1, and k_2. The physical meaning of Ge is important, representing the *ratio* of the tube driving force to the resistance forces occurring in the viscometer [2]. A large Ge means that a large driving force is required to drive the tube to reach a certain velocity. Figure 2 shows $1/\mathrm{Ge}_i$ as a function of k_1 and k_2 and can be used to approximately choose the proper viscometer geometry for a particular design. It can be seen from the figure that the falling cylinder viscometer is a special case of the FTV as $k_1 = 0$. For each curve in the figure, there is one point where the slope is zero. This means that the geometry number is less sensitive to k_2. For tubes with $k_1 = 0.48$ and $k_2 = 0.67$, the geometry number is less sensitive to both k_1 and k_2. This characteristic can be used to improve the accuracy of the FTV.

The Actual or Correct Model

The actual geometry number can be derived from the force balance equation and written as the following if the flow field around the tube is known.

$$\mathrm{Ge} = \frac{1}{l^+(k_2^2 - k_1^2)}\left\{\mathrm{Re}_{R_s}\int_{k_1}^{k_2}r^+(p_{x_A^+}^+ - p_{x_B^+}^+)\,dr^+\right.$$

$$\left. +2\int_{x_A^+}^{x_B^+}\left[-k_1\left(\frac{\partial u^+}{\partial r^+}\right)_{k_1} + k_2\left(\frac{\partial u^+}{\partial r^+}\right)_{k_2}\right]dx^+\right\}. \quad (3b)$$
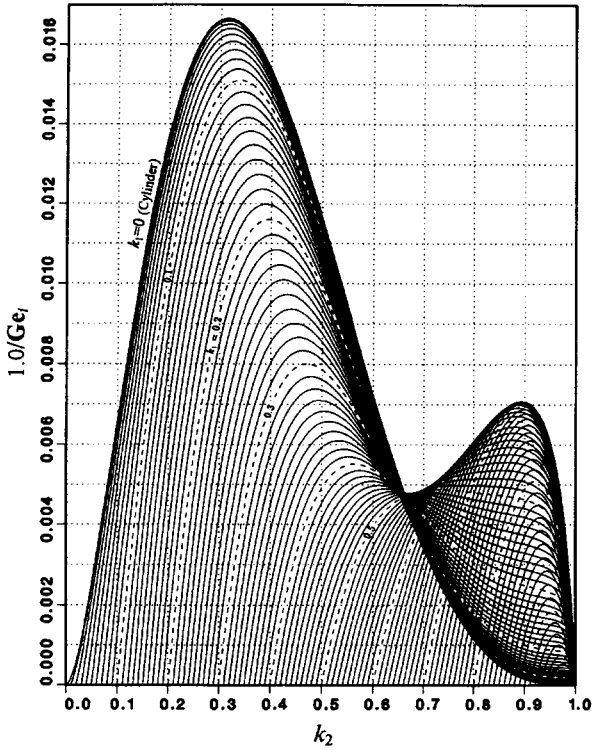
Figure 2. Reciprocal of ideal geometry number.

This geometry number must satisfy the equation

$$Ge = \frac{(\rho_t - \rho_f)gR_s^2}{\mu u_t}.$$ (4b)

Equation (4b) can be used directly either to evaluate the actual Ge experimentally or measure the fluid viscosity if the Ge value is known.

The flow in the FTV is unsteady. However, by using a moving coordinate system as shown in Fig. 3, the flow is converted into a steady one, simplifying the problem significantly. In the moving coordinate system, the tube is stationary and the fluid approaches the tube with the terminal velocity u_t. The dimensionless momentum and continuity equations have the form

$$\frac{\partial(u^+u^+)}{\partial x^+} + \frac{1}{r^+}\frac{\partial(u^+v^+r^+)}{\partial r^+}$$
$$= -\frac{1}{2}\frac{\partial p^+}{\partial x^+} + \frac{1}{Re_{R_s}}$$
$$\times \left[\frac{\partial^2 u^+}{\partial x^{+2}} + \frac{1}{r^+}\frac{\partial}{\partial r^+}\left(r^+\frac{\partial u^+}{\partial r^+}\right)\right],$$ (5)

$$\frac{\partial(u^+v^+)}{\partial x^+} + \frac{1}{r^+}\frac{\partial(v^+v^+r^+)}{\partial r^+}$$
$$= -\frac{1}{2}\frac{\partial p^+}{\partial r^+} + \frac{1}{Re_{R_s}}$$
$$\times \left[\frac{\partial^2 v^+}{\partial x^{+2}} + \frac{1}{r^+}\frac{\partial}{\partial r^+}\left(r^+\frac{\partial v^+}{\partial r^+}\right) - \frac{v^+}{r^{+2}}\right],$$ (6)
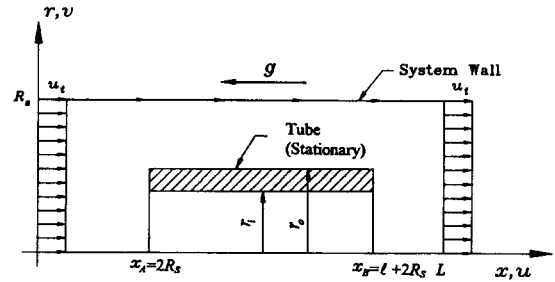

Figure 3. Coordinate system moving with the tube.

$$\frac{\partial u^+}{\partial x^+} + \frac{1}{r^+}\frac{\partial(v^+r^+)}{\partial r^+} = 0,$$ (7)

with boundary conditions

$$u^+(0,r^+) = 1.0, \qquad v^+(0,r^+) = 0,$$
$$u^+(L^+,r^+) = 1.0, \qquad v^+(L^+,r^+) = 0,$$
$$u^+(x^+,1.0) = 1.0, \qquad v^+(x^+,1.0) = 0,$$
$$\frac{\partial u^+}{\partial r^+}(x^+,0) = 0, \qquad v^+(x^+,0) = 0,$$
$$u^+(x_A^+, k_1 \le r^+ \le k_2) = 0,$$
$$v^+(x_A^+, k_1 \le r^+ \le k_2) = 0,$$ (8)
$$u^+(x_B^+, k_1 \le r^+ \le k_2) = 0,$$
$$v^+(x_B^+, k_1 \le r^+ \le k_2) = 0,$$
$$u^+(x_A^+ \le x^+ \le x_B^+, k_1) = 0,$$
$$v^+(x_A^+ \le x^+ \le x_B^+, k_1) = 0,$$
$$u^+(x_A^+ \le x^+ \le x_B^+, k_2) = 0,$$
$$v^+(x_A^+ \le x^+ \le x_B^+, k_2) = 0.$$

A Fortran program using the SIMPLE algorithm [29, 30] was developed to solve the momentum and continuity equations simultaneously for the velocity and pressure fields. The solution was obtained progressively by iteration [2]. For each particular geometry and Reynolds number, the program ends up with three matrices: the axial velocity, the radial velocity, and the pressure. The geometry number can then be calculated numerically from Eq. (3b), according to the shear stresses and pressure drags determined from the solution matrices.

To produce a final working equation for the viscometer, an often used term, the *end correction factor* (ECF), is introduced. It is defined as the ratio of the actual to the ideal geometry numbers. The ECF physically represents the deviation of an actual model from its corresponding ideal model.

$$ECF = Ge/Ge_i.$$ (9a)

The alternative form of the equation, which is convenient for the Ge calculation, is

$$Ge = ECF \, Ge_i.$$ (9b)

There is a great advantage to the ECF. The value of Ge

extends over several orders of magnitude, but the ECF is usually between 1.0 and 1.10. If the ECF as a function of k_1, k_2, and l^+ can be found, then the actual value of Ge can be readily determined because the ideal geometry number can be calculated from Eq. (4a).

COMPUTATIONAL RESULTS

Nature of the End Effect

To illustrate the nature of the end effect, the detailed solution for an actual FTV with $k_1 = 0.47453$, $k_2 = 0.52393$, $l^+ = 5.5929$, and $\mathrm{Re}_{R_s} = 0.01716$ is used as an example. Figure 4 shows a velocity vector diagram of this actual FTV. For a clear view of the velocity field near the tube ends, the width of the graph and the velocity components in the r^+ direction have been enlarged by a factor of 2.4. Fluid flows through both the inside and outside passages. Similar but different diagrams are presented in the Appendix in Figs. A1 and A2 for two tubes with a smaller or larger diameter and a thicker wall. There is no upward flow inside the smaller tube in Fig. A1 and no upward flow outside the larger tube in Fig. A2.

Figure 5 shows the variation of the wall shear rate along the tube walls. For comparison, the shear rates for the ideal model are also indicated in the figure by dotted lines. The end shear rates are large, but they quickly decay to the value corresponding to the ideal case. The significant increase in shear rate near the tube ends
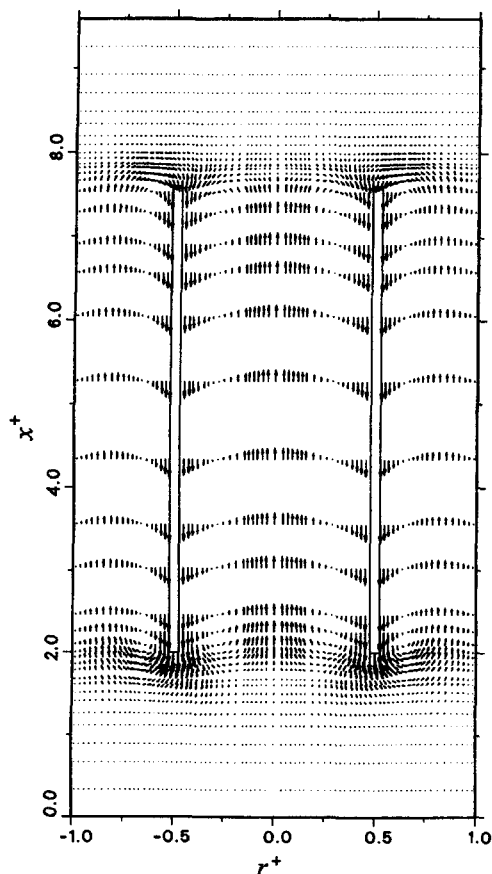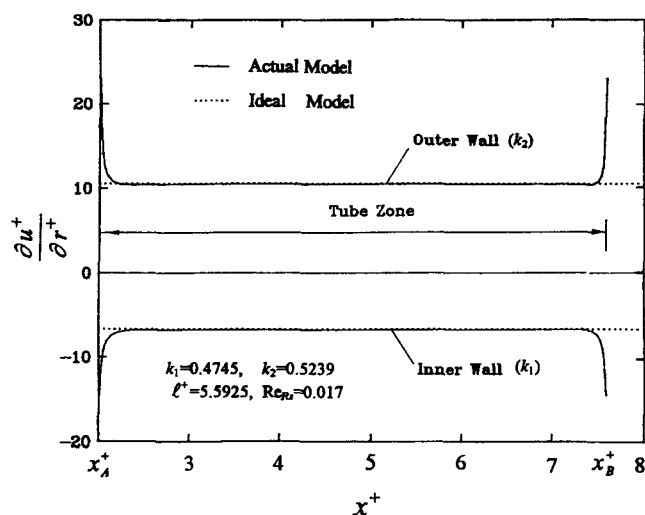

Figure 5. Shear rate variation on the tube walls.

makes Ge increase from its ideal counterpart. The dimensionless length of the transition region is approximately equal to 0.17 on both ends. These results agree well with the flow visualization results of Kim et al. [22] on the falling needle viscometer. It was found that these end shear rate variations remain essentially the same for shorter or longer tubes. This suggests that the end effects of shear stress on the geometry number are smaller for longer tubes.

Computational results also revealed another important fact. If the pressure distribution in the radial direction is plotted for $x^+ = x_A^+$ where the tube forward end is located, a sharp step pressure increase occurs at the tube forward end. Similarly, there is a sharp step pressure decrease at the tube back end [2]. This means that the tube ends encounter a higher or lower pressure than their corresponding pressures in the ideal model. Curve B in Fig. 6 shows the pressure variation in the x^+ direction for $r^+ = 0.48$ passing through the tube wall. Curves A and C display the pressure distribution for $r^+ = 0.31$ and 1.0, respectively; one is inside the tube and the other is on the container wall. These two curves are very close to the ideal case (not shown in the figure). The large pressure increase and decrease at the tube ends can be seen clearly by taking pressure readings at x_A^+ and x_B^+ from Fig. 6.

The pressure increase and decrease at the tube ends can be significant compared with the total pressure drop across the tube in the ideal case. This leads to an actual total pressure drop across the tube 48% larger than in the ideal case for this k_1, k_2 pair. However, the contribution of this additional pressure drop to Ge is no more than a few percent (3.527% in this case) for thin-walled tubes due to the relatively small influence of the pressure drop on Ge. Table 1 gives quantitatively the shear and pressure differences between the ideal and actual (numerically computed) results and their effects on the geometry number. The difference in the geometry number values between the numerical and ideal results is the end effect. It is seen from the table that the geometry number increases by 5.539%, up to 400.88 from 379.84. In general, the increase in pressure drop accounts for two-thirds of the total end effects on the geometry number.
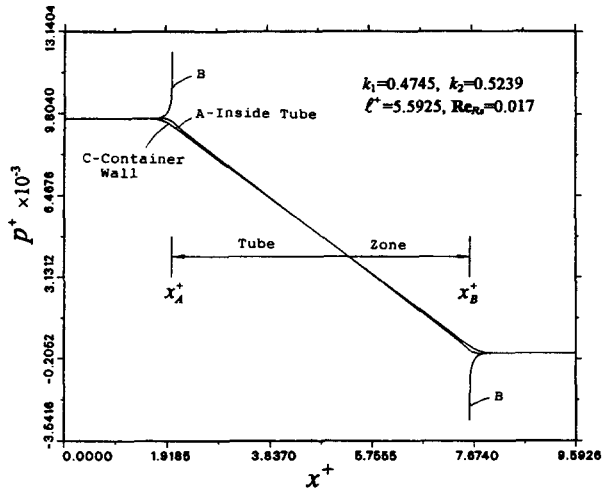

Figure 4. Diagram of velocity vectors in the FTV.

Figure 6. Pressure increase and decrease on tube ends.

Geometry Number and End Correction Factor

A series of calculations were conducted for a variety of FTVs to investigate the variation of the geometry number and ECF with tube configuration. Tables 2 and 3 show the results of the calculations, listing the Ge_n and ECF, respectively, for various values of k_1 and k_2 as $l^+ = 10.0$, a convenient length experimentally, and $Re_{R_s} = 10^{-6}$, a small Reynolds number to suppress inertial forces. Graphical results from the tables are presented in Fig. 7, where the abscissa is the dimensionless central radius. Curves are plotted for constant wall thickness, $\delta = k_2 - k_1$. The solid lines are the Ge_n, and the dashed lines represent the ECF. For all wall thicknesses, Ge_n has the largest values around $(k_1 + k_2)/2 = 0.55$ while the ECFs have the smallest values in the vicinity of $(k_1 + k_2)/2 = 0.52$.

In the calculations, the Reynolds number was taken to be small (10^{-6}); therefore the flow could be considered to be Stokesian. It is of great operational interest to determine the maximum Reynolds number for which the present analysis is applicable. This was done by increasing the Reynolds number, calculating the geometry number, and comparing it with the geometry number at a Reynolds number of 10^{-6}. Figure 8 shows the results of such calculations where the ordinate is defined as

$$Ge^+ = \frac{GeRe_{R_s}}{Ge \times 10^{-6}} \qquad (10)$$

Table 1. Contribution of Shear Force and Pressure[a] to Ge

Item	Ideal Result	Numerical Result	Difference	Effect on Ge
Inner shear force contribution to Ge	127.25	132.58	4.19%	1.405%
Outer shear force contribution to Ge	224.73	227.03	1.026%	0.607%
Pressure force contribution to Ge	27.87	41.27	48.06%	3.527%
Total contribution to Ge	379.84	400.88	5.54%	5.539%

[a] Tube parameters: $k_1 = 0.4745$, $k_2 = 0.5239$, $l^+ = 5.5925$, and $Re_{R_s} = 0.017$.

where Ge^+ is the normalized geometry number with respect to the Ge at $Re_{R_s} = 10^{-6}$. Also presented in the figure are the results for FCV where the k_1's are equal to zero [1]. The value of Ge^+ provides information on the inertial effect. As seen in the figure, the present model is applicable to a Reynolds number up to 5.0. For larger values of the Reynolds number, the inertial effects are significant. The inertial forces come into play earlier for thinner wall tubes. At $Re_{R_s} = 50$, where additional resistance due to the inertial forces becomes apparent, the geometry numbers increase by 1.0%. The experimental results in Fig. 8 will be discussed later.

EXPERIMENTAL APPARATUS

Experiments were performed to investigate the stability, reproducibility, and accuracy of the FTV. The experimental results were used to verify the theoretical results. Measurements were carried out on a number of falling tubes of different geometries and densities to investigate the characteristics of the FTV. The experimental apparatus included a container, a series of falling tubes, and peripheral facilities that either provided constant temperature in the system or measured the falling time.

A schematic of the apparatus is shown in Fig. 9, which is similar to that used for previous experiments on the FCV [1]. The only difference is the replacement of the cylinders with tubes.

The tubes were made of glass or plastics with a heavy metal ring of the same diameter at the bottom to lower the center of gravity. Once a tube is dropped into the launcher, it will fall due to gravity. At low Reynolds

Table 2. Numerically Obtained[a] Geometry Numbers (Ge_n)

δ $(k_2 - k_1)$	$(k_1 + k_2)/2$					
	0.3	0.4	0.5	0.6	0.7	0.8
0.02	504.088	671.323	859.635	930.639	842.361	759.618
0.05	222.228	299.627	390.698	424.620	378.954	338.593
0.10	130.790	180.580	242.950	266.100	231.450	203.900
0.15	102.925	145.892	203.192	224.537	189.784	165.532
0.20	91.400	133.280	193.080	215.690	176.450	153.691
0.30	86.429	134.681	214.707	246.338	185.620	175.707

[a] According to $l^+ = 10$ and $Re_{R_s} = 10^{-6}$.

Table 3. Numerically Obtained[a] End Correction Factors (ECF$_n$)

δ $(k_2 - k_1)$	$(k_1 + k_2)/2$					
	0.3	0.4	0.5	0.6	0.7	0.8
0.02	1.06577	1.05251	1.03466	1.03975	1.05706	1.06227
0.05	1.06553	1.05200	1.03681	1.04290	1.06048	1.06620
0.10	1.06400	1.05115	1.03805	1.04570	1.06376	1.06981
0.15	1.06235	1.05008	1.03791	1.04638	1.06535	1.07130
0.20	1.06028	1.04799	1.03649	1.04581	1.06576	1.07081
0.30	1.05522	1.04439	1.03351	1.04324	1.06422	1.06171

[a] According to $l^+ = 10$ and $\mathrm{Re}_{R_s} = 10^{-6}$.

numbers, the tube only requires a distance less than one container diameter to reach its (constant) terminal velocity [22, 31, 32]. A magnet fixed at the bottom of the tubes triggers a timer via a Hall magnetic sensor and then stops the timer as it passes another sensor. The terminal velocity can then be calculated by dividing the distance between the successive sensors by the falling time recorded on the timer.

To determine the general characteristics of the FTV, three series of a total of 16 tubes were tested. The specifications of the experimental tubes and their ideal geometry number are listed in Table 4.

The major parts of the tubes in series TA were made out of precision glass tubes from the Fisher Scientific Company. Those in series TB and TC were made out of standard plastic tubes. The tubes in series TA have the same diameter and density but different lengths and therefore were used to determine the length effect. To investigate the inertial effect, tubes TB1–TB9 have approximately the same diameter and length but different densities. Tubes TB10–TB12 are similar to those in series TA but with thicker walls. Note that there are slight differences of Ge_i between tubes in TB series due to small diameter differences in the stock tubes. Tube TC1 has the smallest diameter. The tests on those tubes with approximately the same length but different diameters were made to investigate the primary characteristic, the variation of Ge with diameter.

The tube diameters were measured by either a vernier or a digital micrometer. The former had a scale increment of 2.5×10^{-5} m and, with careful reading, an accuracy of 10^{-5} m. The latter had a resolution of 10^{-6} m.
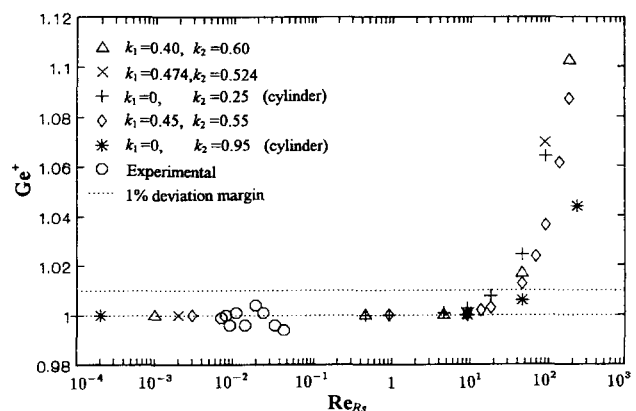
The tube densities were determined by weighing them in air and distilled water. The accuracy of the density measurements was estimated to be ± 0.0001 g/cm^3 with a repeatability of 0.005% [2].

EXPERIMENTAL RESULTS

As long as the center of buoyancy for a tube is above the center of gravity and the dimensionless tube outer diameter is less than 0.75, the falling tube is stable and remains in the center in a vertical position as it falls through the test fluid. When k_2 is greater than 0.75, the tubes tend to become unstable and drift toward the container wall.

Viscosities were measured between 1200 and 1400 cP using standard fluids from the Cannon Standard Instrument Company (State College, PA) specified to be accurate within 1%. Since one of the primary purposes of the experiments was to verify the calculated geometry numbers, it was desirable to suppress all other possible errors. Thus the standard fluid viscosities were selected to have slowly falling tubes in order to have less error in the total falling time.

The experimental geometry numbers and ECFs were obtained from Eqs. (4b) and (9a), respectively. These results can be compared with the numerical results to determine the accuracy of the FTV. Another way to verify

Figure 7. Numerically calculated geometry numbers and end correction factors.

Figure 8. Effect of Reynolds number on geometry number.

1. System (Cylindrical Container)
2. Falling Tube
3. Fluid to be Measured
4. 4-Wire RTD
5. Tube Launcher
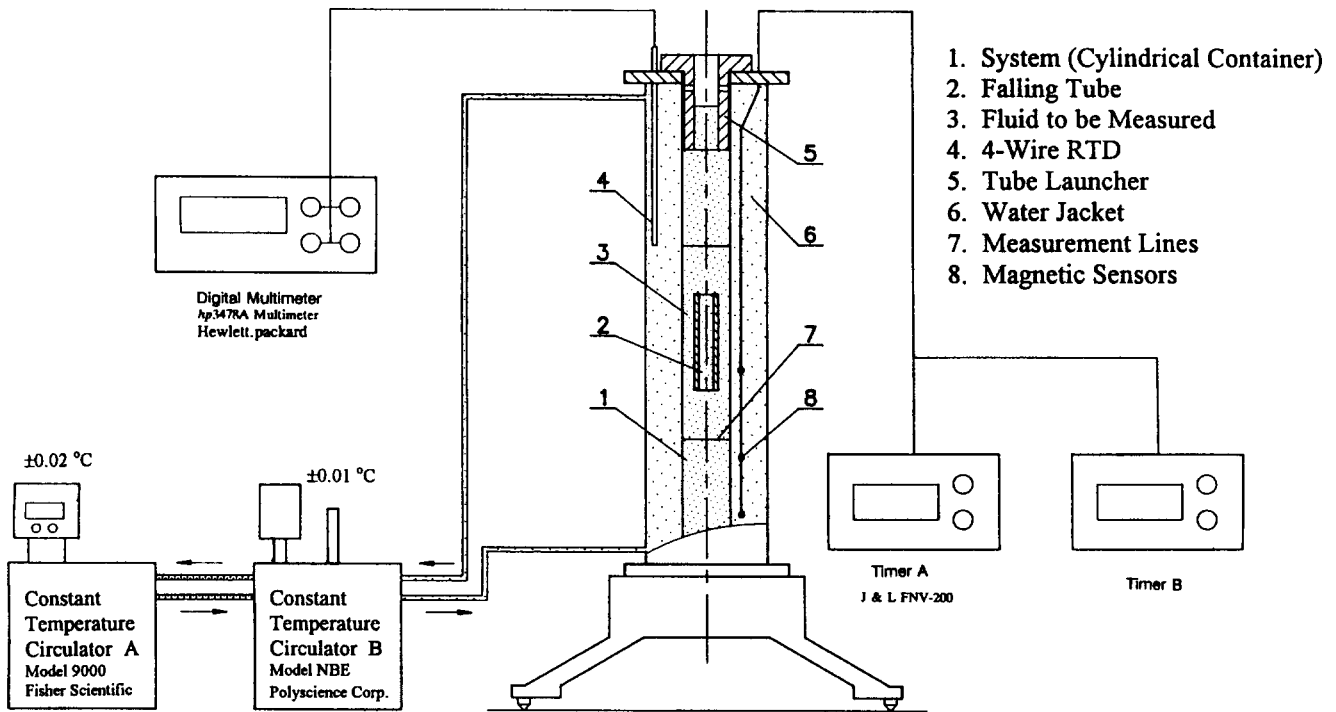6. Water Jacket
7. Measurement Lines
8. Magnetic Sensors

Figure 9. Schematic of experimental apparatus of the falling tube viscometer.

the experimental and numerical results is to examine the normalized viscosity defined as

$$\mu^+ = \frac{\mu_m}{\mu_s} = \frac{(\rho_t - \rho_f)gR_s^2}{\mu_s u_t Ge_n} = \frac{Ge_e}{Ge_n}. \qquad (11)$$

Since both the numerical geometry number and the measured tube terminal velocity were used in viscosity calculations, μ^+ can be used to indicate the accuracy of the numerical as well as the experimental results. Any errors

in either calculations or experiments will make the normalized viscosity deviate from unity.

Tables 5 and 6 compare the results of the numerical analysis and experiments, showing the Reynolds numbers, the calculated and experimental geometry numbers, the measured viscosities, and the normalized viscosity.

DISCUSSION OF EXPERIMENTAL RESULTS

As seen from Tables 5 and 6, the agreement between the calculated and measured geometry numbers is better than

Table 4. Specifications of the Experimental Falling Tubes[a]

Tube	d_i (mm)	d_o (mm)	l (mm)	k_1	k_2	l^+	Ge_i	ρ_t (kg/m³)
TA1	9.040	9.981	53.27	0.4745	0.5239	5.593	379.87	2594.2
TA2	9.040	9.981	96.11	0.4745	0.5239	10.09	379.87	2548.2
TA3	9.040	9.981	175.8	0.4745	0.5239	18.46	379.87	2583.2
TB1	9.62	12.71	99.98	0.5050	0.6672	10.50	212.35	1236.6
TB2	9.58	12.70	100.6	0.5029	0.6667	10.56	212.05	1285.2
TB3	9.62	12.70	100.0	0.5050	0.6667	10.50	212.51	1336.6
TB4	9.62	12.69	100.0	0.5050	0.6661	10.50	212.67	1434.6
TB5	9.61	12.70	100.1	0.5045	0.6667	10.51	212.39	1585.5
TB6	9.59	12.70	100.2	0.5034	0.6667	10.52	212.16	1837.1
TB7	9.61	12.69	100.4	0.5045	0.6661	10.54	212.55	2083.4
TB8	9.65	12.68	101.1	0.5066	0.6656	10.61	212.22	2603.3
TB9	9.64	12.70	100.2	0.5060	0.6667	10.52	212.75	3083.5
TB10	9.61	12.70	40.28	0.5045	0.6667	4.229	212.39	1435.3
TB11	9.62	12.69	100.0	0.5050	0.6661	10.50	212.67	1434.3
TB12	9.61	12.70	200.7	0.5045	0.6667	21.07	212.39	1454.8
TC1	8.60	10.52	95.40	0.4514	0.5522	10.02	233.99	1431.4

[a] System diameter = 19.05 mm.

Table 5. Comparison of Experimental and Numerical Results[a] TA and TC Series

Tube	d_f (mm)	Δt (s)	Re_{R_s}	Ge_e	Ge_n	$(\mathrm{Ge}_n/\mathrm{Ge}_e) - 1$	μ_m (cP)	μ^+
TA1	100	36.15	.017	403.13	400.88	−0.56%	1367.1	1.0056
TA1	100	36.01	.017	401.57	400.88	−0.17%	1361.8	1.0017
TA1	100	36.01	.017	401.57	400.88	−0.17%	1361.8	1.0017
TA1	100	35.91	.017	400.46	400.88	+0.11%	1358.1	0.9989
TA1	100	36.04	.017	401.91	400.88	−0.26%	1363.0	1.0026
TA1	100	35.89	.017	400.23	400.88	+0.16%	1357.3	0.9984
Avg.	100	36.00	.017	401.48	400.88	−0.15%	1361.5	1.0015
TA2	100	36.34	.017	394.32	393.79	−0.13%	1361.3	1.0013
TA2	100	36.18	.017	392.58	393.79	+0.31%	1355.3	0.9969
TA2	100	36.11	.017	391.82	393.79	+0.50%	1352.7	0.9950
TA2	100	36.08	.017	391.49	393.79	+0.59%	1351.6	0.9942
TA2	100	36.14	.017	392.15	393.79	+0.42%	1353.8	0.9958
TA2	100	36.25	.017	393.34	393.79	+0.11%	1357.9	0.9989
Avg.	100	36.18	.017	392.62	393.79	+0.30%	1355.5	0.9970
TA3	90	31.42	.018	386.80	386.95	+0.04%	1359.0	0.9996
TA3	90	31.36	.018	386.07	386.95	+0.23%	1356.4	0.9977
TA3	90	31.45	.018	387.17	386.95	−0.06%	1360.3	1.0006
TA3	90	31.44	.018	387.05	386.95	−0.03%	1359.9	1.0003
TA3	90	31.36	.018	386.07	386.95	+0.23%	1356.4	0.9977
TA3	90	31.44	.018	387.05	386.95	−0.03%	1359.9	1.0003
Avg.	90	31.41	.018	386.70	386.95	+0.06%	1358.6	0.9994
TC1	100	71.89	.008	241.43	242.68	+0.52%	1418.7	0.9949
TC1	100	72.17	.008	242.37	242.68	+0.13%	1424.2	0.9987
TC1	100	71.97	.008	241.70	242.68	+0.40%	1420.3	0.9960
TC1	100	71.94	.008	241.60	242.68	+0.45%	1419.7	0.9956
TC1	100	71.66	.008	240.66	242.68	+0.84%	1414.1	0.9917
TC1	100	71.75	.008	240.96	242.68	+0.71%	1415.9	0.9929
Avg.	100	71.90	.008	241.46	242.68	+0.51%	1418.8	0.9950

[a] For TA series, $\rho_f = 889.47$ kg/m³ and $\mu_s = 1359.5$ cP. For TC series, $\rho_f = 892.90$ kg/m³ and $\mu_s = 1426.0$ cP. The local acceleration of gravity is 9.8024 m/s².

Table 6. Comparison of Experimental and Numerical Results[a] TB Series

Tube	d_f (mm)	Δt (s)	Re_{R_s}	Ge_e	Ge_n	$(\mathrm{Ge}_n/\mathrm{Ge}_e) - 1$	μ_m (cP)	μ^+
TB1	100	93.11	0.007	220.04	221.29	+0.57%	1282.7	0.9943
	100	93.91	0.007	221.93	221.29	−0.29%	1293.7	1.0029
TB2	100	81.75	0.008	220.58	220.97	+0.18%	1287.7	0.9982
	100	81.95	0.008	221.12	220.97	−0.07%	1290.9	1.0007
TB3	100	72.08	0.009	220.03	221.45	+0.64%	1281.7	0.9936
	100	72.48	0.009	221.25	221.45	+0.09%	1288.9	0.9991
TB4	100	59.47	0.011	221.72	221.62	−0.04%	1290.6	1.0004
	100	59.48	0.011	221.75	221.62	−0.06%	1290.8	1.0006
TB5	100	46.33	0.014	220.93	221.33	+0.18%	1287.6	0.9982
	100	46.15	0.014	220.07	221.33	+0.57%	1282.6	0.9943
TB6	100	34.14	0.019	222.02	221.09	−0.42%	1295.4	1.0042
	100	34.11	0.019	221.82	221.09	−0.33%	1294.3	1.0033
TB7	100	27.03	0.024	221.68	221.49	−0.08%	1291.1	1.0008
	100	27.06	0.024	221.92	221.49	−0.19%	1292.5	1.0019
TB8	100	18.73	0.035	220.74	222.20	+0.66%	1281.5	0.9934
	100	18.88	0.035	222.51	222.20	−0.14%	1291.8	1.0014
TB9	100	14.61	0.045	220.55	221.71	+0.53%	1283.3	0.9948
	100	14.58	0.045	220.10	221.71	+0.73%	1280.6	0.9927
TB10	150	103.0	0.009	232.28	232.17	−0.05%	1426.7	1.0005
TB11	200	131.3	0.009	221.66	221.46	−0.09%	1427.3	1.0009
TB12	100	61.50	0.010	215.52	216.58	+0.49%	1419.0	0.9951

[a] For tubes TB1–TB9, $\rho_f = 893.81$ kg/m³ and $\mu_s = 1290.0$ cP. For tubes TB10–TB12, $\rho_f = 892.90$ kg/m³ and $\mu_s = 1426.0$ cP. The local acceleration of gravity is 9.8024 m/s².

±1.0% and usually better than ±0.5%. This is essentially the same as the agreement between the measured and standard viscosities.

Reproducibility of the viscosity measurements was investigated with the tubes in series TA. Six runs were made for each tube. The normalized viscosities in Table 5 are presented graphically in Fig. 10. It is seen that the reproducibility for all runs is ±0.5%.

The geometry number is mainly determined by k_1 and k_2 rather than l^+. However, the deviation of the geometry number from its corresponding ideal geometry number, i.e., the ECF, is very sensitive to l^+. Figure 11 illustrates the effect of tube length on the ECF with tubes TB10–TB12. These tubes have dimensionless lengths of 4.229, 10.50, and 21.07, respectively, but nearly the same k_1, k_2, and Ge_i, (Table 4). As l^+ increases, the viscometer approaches the ideal model, Ge approaches Ge_i, and therefore ECF converges to unity. The value of (ECF-1) for a particular pair of k_1 and k_2 is approximately inversely proportional to the tube length. Considering this factor and other factors such as inconvenience, it is recommended that $l^+ = 10$ is a suitable value for the falling tubes.

The data of tubes TB1–TB9 show that the effect of the Reynolds number on the geometry number is small. No apparent variation was observed as the Reynolds number increased from 0.0071 to 0.0452. These experimental data are shown in Fig. 8 as circles along with calculated values from the numerical analysis.

ERROR ANALYSIS

A detailed error analysis of the experiments was conducted on the geometry number [2]. Possible errors were considered in the falling time and distance, tube and fluid densities, container and tube diameters, container inclination, falling stability, tube eccentricity, and temperature variations. It was predicted that the overall experimental errors were 0.5–1.5%. These are somewhat larger than the results of the experiments on the standard fluids, which were well within 1.0%.

CORRELATION EQUATIONS

One of the problems with numerical solutions is that the result is a plethora of numbers that many times are not
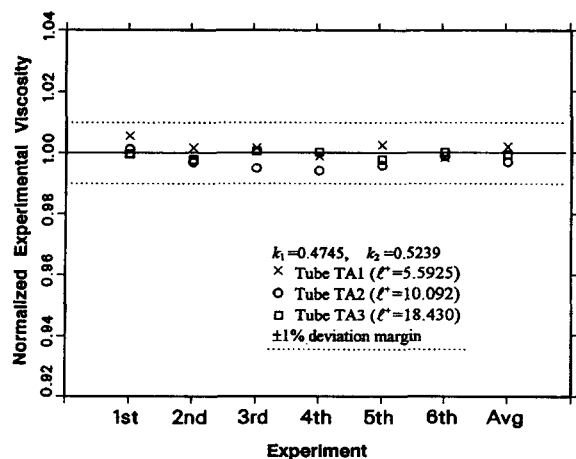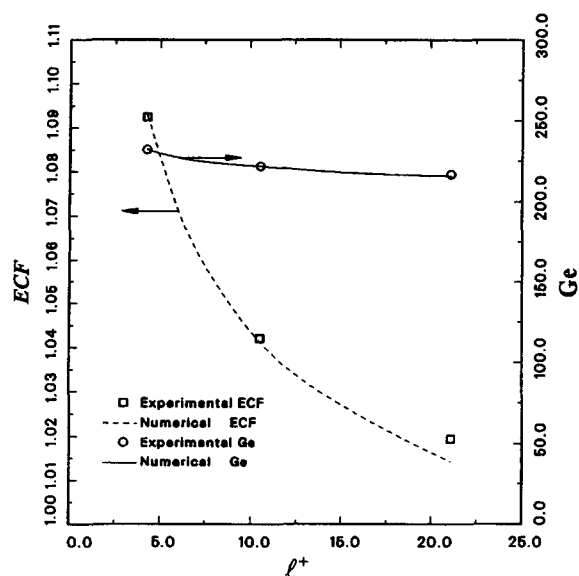

Figure 11. Effect of tube length on ECF (TB10–TB12).

continuous over sufficiently small increments of the field. This is true for the present solution, where it is difficult to determine, from a group of limited numerical results, the geometry number or the ECF for arbitrary values of the parameters k_1, k_2, and l^+. From a design point of view, a correlated equation in terms of the three parameters k_1, k_2, and l^+ would be convenient and sufficient. The Reynolds number was not included because of its negligible effect at small values but may be regressed independently with good approximation if large Reynolds numbers are unavoidable.

Taking advantage of its small variation, the ECF was chosen to be correlated. The correlated equation of the ECF for the special case of the FTV, the FCV, was previously reported in [1]. For general FTVs, the following correlation form was found to be appropriate.

$$ECF = 1 + \alpha(k_1, k_2)\beta(l^+), \qquad (12)$$

where α is the contribution of the tube diameters and β the contribution of the tube lengths. Using the data in Tables 3–6, a matrix equation for α can be written as

$$\alpha = D \cdot A \cdot T, \qquad (13)$$

where D is the tube diameter vector, A the coefficient matrix, and T the tube wall thickness vector.

$$D = |1, k_1 + k_2, (k_1 + k_2)^2, (k_1 + k_2)^3, (k_1 + k_2)^4|,$$

$$A = \begin{vmatrix} -0.5762 & 3.6889 & -20.0268 & 29.0440 \\ 2.9353 & -15.4479 & 83.2855 & -120.494 \\ -4.7164 & 22.7371 & -123.105 & 176.454 \\ 3.1158 & -13.9315 & 75.9630 & -107.009 \\ -0.7246 & 3.0570 & -16.7378 & 22.9341 \end{vmatrix},$$

and

$$T = \begin{vmatrix} 1.0 \\ k_2 - k_1 \\ (k_2 - k_1)^2 \\ (k_2 - k_1)^3 \end{vmatrix} \quad \text{for } k_1 + k_2 < 1.6 \text{ and } k_2 - k_1 < 0.3.$$

Figure 10. Reproducibility and accuracy of FTV.

Table 7. Comparison of Correlated and Experimental ECFs

Tube	k_1	k_2	l^+	ECF_e^a	ECF_r	$(ECF_r - ECF_e/ECF_e)$
TA1	0.4745	0.5239	5.593	1.05688	1.06382	+0.66%
TA2	0.4745	0.5239	10.09	1.03355	1.03736	+0.37%
TA3	0.4745	0.5239	18.46	1.01798	1.02006	+0.20%
TB1	0.5050	0.6672	10.50	1.04066	1.04178	+0.11%
TB2	0.5029	0.6667	10.56	1.04153	1.04137	−0.02%
TB3	0.5050	0.6667	10.50	1.03827	1.04175	+0.33%
TB4	0.5050	0.6661	10.50	1.04263	1.04171	−0.09%
TB5	0.5045	0.6667	10.51	1.03817	1.04168	+0.34%
TB6	0.5034	0.6667	10.52	1.04600	1.04155	−0.43%
TB7	0.5045	0.6661	10.54	1.04352	1.04153	−0.19%
TB8	0.5066	0.6656	10.61	1.03939	1.04141	+0.19%
TB9	0.5060	0.6667	10.52	1.03558	1.04176	+0.60%
TB10	0.5045	0.6667	4.229	1.09364	1.09594	+0.21%
TB11	0.5050	0.6661	10.50	1.04229	1.04171	−0.06%
TB12	0.5045	0.6667	21.07	1.01471	1.01897	+0.42%
TC1	0.4514	0.5522	10.02	1.03191	1.03885	+0.67%

[a] Average values were used for ECF_e except for tubes TB10–TB12.

An alternative algebraic equation for α is also given in the Appendix as Eq. (A1). The correlated equation for β as a function of l^+ is

$$\beta = \begin{cases} \dfrac{10}{l^+}[1 + 0.00963(l^+ - 10) - 8.015 \times 10^{-4}(l^+ - 10)^2 \\ \qquad\qquad -6.737 \times 10^{-5}(l^+ - 10)^3] \quad \text{for } l^+ < 20, \\[2mm] \dfrac{10.052}{l^+} - 0.0293 \qquad \text{for } 20 \le l^+ \le 50. \end{cases}$$

(14)

The error introduced by the correlation is small (less than 0.25%), but the convenience is great. To verify the accuracy of the correlated equation directly with the experimental results, the correlation equation, Eq. (12), was applied to the tested tubes listed in Table 4. The results are shown in Table 7. The agreement is good, and all of the differences are well within ±1.0%.

SELECTION OF SYSTEM GEOMETRY

A small geometry number will result in a large Reynolds number if the density difference between the tube and fluid is large enough. In order to have a moderate falling time and no apparent inertial effect, a appropriate geometry number must be selected. There exists a range of geometry numbers that satisfy both constraints.

It is known from Fig. 8 that if the Reynolds number is less than 5.0, there are no appreciable inertial effects. The maximum allowed Re_{R_s} is approximately 10 if a 0.25% deviation of Ge is permissible. Therefore, from Eq. (4b) and the definition of the system Reynolds number, the minimum value of Ge to avoid significant inertial effects is

$$Ge_{min} \ge \frac{\rho_f(\rho_t - \rho_f)gR_s^3}{10\mu^2}.$$

(15)

From a manufacturing point of view, the system radius R_s may be chosen to be around 1.0 cm and the length of the container around $40R_s$. Special attention should be

given to the value selected for the tube density. Although it is natural to think that the tube density could be chosen just slightly higher than the fluid density to allow the tube to fall slowly, this can lead to errors because the tube and fluid densities enter into the equation as a *density difference*. This important characteristic should be kept in mind in choosing a tube density. It is recommended that the tube density be at least 0.05 g/cm³ larger than the fluid density. In this way, the error in the measured viscosity due to the error in density difference will be less than 0.4% if the densities have an accuracy of 0.0001 g/cm³.

The geometry numbers are largely determined by the tube cross-sectional dimensions. By referring to Fig. 2, many pairs of k_1 and k_2 can be selected for a given value of Ge. The values of k_1 and k_2 should be chosen in such a way that the ECF, $\partial Ge/\partial k_1$, and $\partial Ge/\partial k_2$ are all small. In this way, an error in diameter measurement will not result in a large error in the geometry number. However, these values generally will not become small together.

PRACTICAL SIGNIFICANCE

The absolute falling tube viscometer that has been described can measure the dynamic viscosity of Newtonian fluids with an accuracy of ±1.0%. It is structurally simple and cost-effective. Both the theoretical analysis and the experimental verification of the analysis are presented. Correlation equations are given to aid in the design of such viscometers for a variety of applications.

SUMMARY

1. An investigation was carried out on the falling tube viscometer, which has several advantages over the falling cylinder viscometer, the latter being a special case of the former. These advantages include an additional shear surface that is useful in lowering the Reynolds number to avoid inertial effects and the maintenance of the dimensional integrity compared to a hollow cylinder when operating at high pressures.
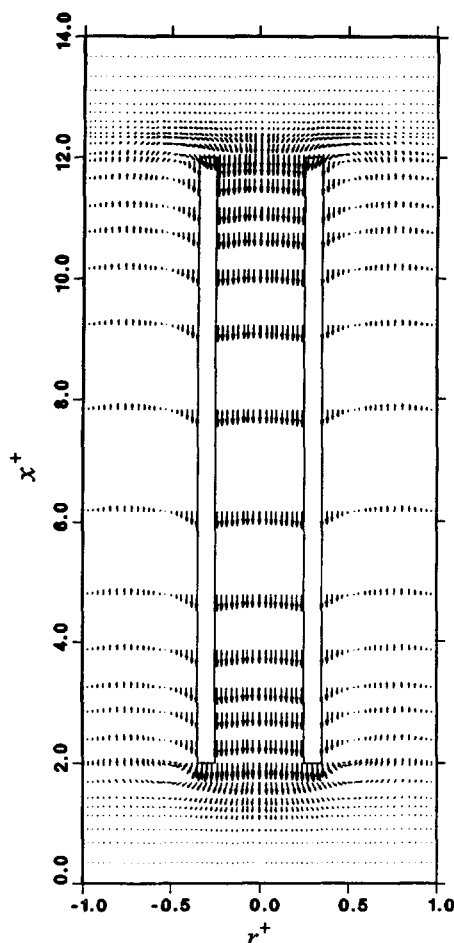
Figure A1. Diagram of velocity vectors in the FTV (smaller diameter tube, $k_1 = 0.25$, $k_2 = 0.35$).
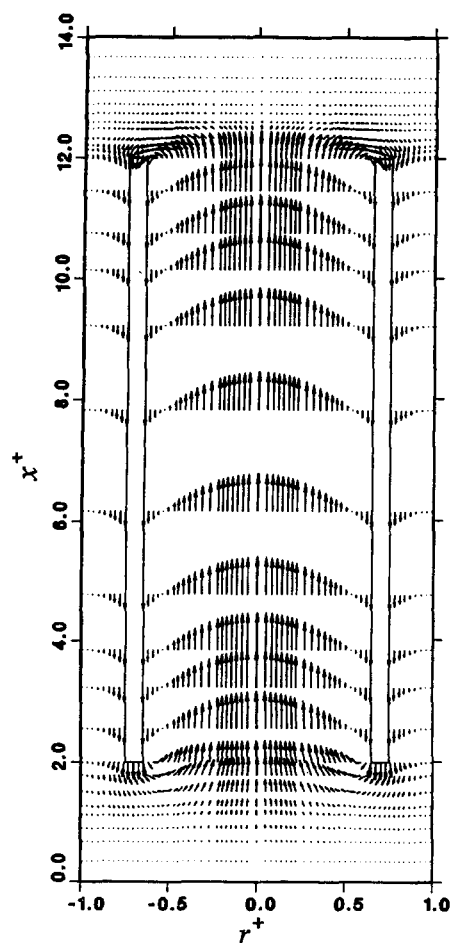

Figure A2. Diagram of velocity vectors in the FTV (larger diameter tube, $k_1 = 0.65$, $k_2 = 0.75$).

2. A dimensionless operational variable, the geometry number (Ge), was defined that represents the ratio of the tube driving force to resistant forces.

3. The falling tube viscometer was analyzed by obtaining a numerical solution of the flow field around the falling tube and the corresponding geometry number. With this information, an end correction factor was determined so that the simple solution for the infinitely long tube could be used to determine the geometry number and fluid viscosities.

4. Experiments were performed to confirm the validity of the numerical solution with the result that measured fluid viscosities were within an accuracy of $\pm 1.0\%$.

5. A generalized solution, a correlation equation of the ECF, was presented for the end correction factor to aid in the design of falling tube viscometers under a variety of operating conditions with an accuracy better than $\pm 1.0\%$.

6. The dimensionless radii k_1 and k_2 can be optimized to minimize the systematic errors.

7. An absolute FTV can therefore be designed with Ge obtained from Ge_i and the correlation equation.

8. Finally, a number of practical suggestions are presented regarding the fluid container, tube lengths, di-

ameters, operational Reynolds numbers, and materials for the most accurate system.

APPENDIX

Figures A1 and A2 show the diagrams of the velocity vectors of the FTV with smaller and larger tube diameters, respectively. A major difference between these two figures and Fig. 4 is that the fluid either inside or outside the tube, depending on the tube size, does not flow upward because of the relatively narrow passage. The parameters of the FTV in Fig. A1 were $k_1 = 0.25$, $k_2 = 0.35$, $l^+ = 10.0$, and $Re_{R_s} = 10^{-6}$, and the parameters in Fig. A2 were $k_1 = 0.65$, $k_2 = 0.75$, $l^+ = 10.0$, and $Re_{R_s} = 10^{-6}$.

For convenience, an alternative algebraic equation for the variable α in Eq. (12) is

$$\alpha = c_1 + c_2(k_1 + k_2) + c_3(k_1 + k_2)^2$$
$$+ c_4(k_1 + k_2)^3 + c_5(k_1 + k_2)^4, \qquad \textbf{(A1)}$$

where

$$c_1 = -0.5762 + 3.6889(k_2 - k_1) - 20.0268(k_2 - k_1)^2$$
$$+ 29.0440(k_2 - k_1)^3,$$

$$c_2 = 2.9353 - 15.4479(k_2 - k_1) + 83.2855(k_2 - k_1)^2$$
$$- 120.494(k_2 - k_1)^3,$$

$$c_3 = -4.7164 + 22.7371(k_2 - k_1) - 123.105(k_2 - k_1)^2$$
$$+ 176.454(k_2 - k_1)^3,$$

$$c_4 = 3.1158 - 13.9315(k_2 - k_1) + 75.9630(k_2 - k_1)^2$$
$$- 107.009(k_2 - k_1)^3,$$

$$c_5 = -0.7246 + 3.05700(k_2 - k_1) - 16.7378(k_2 - k_1)^2$$
$$+ 22.9341(k_2 - k_1)^3.$$

For instance, α should be equal to 0.038978 as $k_1 = 0.45$ and $k_2 = 0.55$.

NOMENCLATURE

d tube diameter, m

d_f tube falling distance, m

ECF   end correction factor (Ge/Ge_i), dimensionless

f Darcy friction factor, (dp^+/dx^+), dimensionless

F_s shear force (see Fig. 1), N

g gravity acceleration, m/s^2

Ge   geometry number $[= (\rho_t - \rho_f)gR_s^2/\mu u_t]$, dimensionless

Ge^+ normalized geometry number, see Eq. (10), dimensionless

k_1 tube inside dimensionless radius $(= r_i/R_s)$, dimensionless

k_2 tube outside dimensionless radius $(= r_o/R_s)$, dimensionless

l tube length, m

l^+ tube length $(= l/R_s)$, dimensionless

L length of calculation domain $(= l + 4R_s$; see Fig. 3), m

L^+ length of calculation domain $(= l^+ + 4)$, dimensionless

P pressure, N/m^2

p pressure causing fluid motion $(= P + \rho_f g)$, N/m^2

p^+ pressure $[= p/(1/2\rho_f u_t^2)]$, dimensionless

R_s system (container) radius, m

r radial coordinate, m

r^+ radial coordinate $(= r/R_s)$, dimensionless

Re_{R_s} Reynolds number based on system radius $(= \rho_f u_f R_s/\mu)$, dimensionless

Δt tube falling time, s

U velocity component in x direction in a stationary coordinate system, m/s

U^+ velocity component in x direction in a stationary coordinate system $(= U/u_t)$, dimensionless

u velocity component in x direction in a moving coordinate system $(= U + u_t)$, m/s

u^+ velocity $(= u/u_t)$, dimensionless

u_t tube terminal velocity $(= d_f/\Delta t)$, m/s

V tube volume, m^3

v velocity component in r direction in a moving coordinate system, m/s

v^+ velocity $(= v/u_t)$, dimensionless

x x coordinate, m

x^+ x coordinate $(= x/R_s)$, dimensionless

Greek Symbols

δ tube wall thickness $(= k_2 - k_1)$, dimensionless

μ viscosity, cP or N s/m^2

μ^+ normalized viscosity, see Eq. (11), dimensionless

ρ density, kg/m^3

Subscripts

A   tube forward (bottom) end

B   tube back (top) end

e   experimental

f   fluid or falling

i   ideal or inside

m   measured

n   numerically computed

o   outside

r   regressed (correlated)

s   system (container) or standard viscosity

t   tube

REFERENCES

1. Gui, F., and Irvine, T. F., Jr., Theoretical and Experimental Study of the Falling Cylinder Viscometer, *Int. J. Heat Mass Transfer*, 37(Suppl. 1), 41–50, 1994,

2. Gui, F., Theoretical and Experimental Study of the Precision Falling Tube Viscometer, Ph.D. Thesis, Mechanical Engineering Dept., State Univ. New York at Stony Brook, NY, 1992.

3. Bridgeman, P. W., The Effect of Pressure on the Viscosities of Forty-Three Pure Liquids, *Proc. Am. Acad. Arts Sci.* **61**, 56, 1926,

4. Lohrenz, J., An Experimental Verified Theoretical Study of the Falling Cylinder Viscometer, Ph.D. Thesis, Univ. Kansas, Lawrence, 1960.

5. Lohrenz, J., Swift, G. W., and Kurata, F., An Experimentally Verified Theoretical Study of the Falling Cylinder Viscometer, *AIChE J.* **6**(4), 547–550, 1960.

6. Ashore, E., Bird, R. B., and Lesearboura, J. A., Falling Cylinder Viscometer for Non-Newtonian Fluids, *AIChE J.* **11**, 910–916, 1965.

7. Eichstadt, F. J., and Swift, G. W., Theoretical Analysis of the Falling Cylinder Viscometer for Power Law and Bingham Plastic Fluids, *AIChE J.* **12**(6), 1179–1183, 1966.

8. Huang, E. T. S., Swift, G. W., and Kurata, F., Viscosity of Methane and Propane at Low Temperature and High Pressure, *AIChE J.* **12**(5), 932–936, 1966.

9. Swift, G. W., Lohrenz, J., and Kurate, F., Liquid Viscosity above Boiling Point for Methane, Ethane, Propane, and *n*-Butane, *AIChE J.* **6**, 415, 1960.

10. Chan, R. K. Y., and Jackson, D. A., Automated Falling-Cylinder High Pressure Laser–Doppler Viscometer, *J. Phys. E: Sci. Instrum.* **18**(6), 510–515, 1985.

11. Kopeliovich, L. V., and Gryaznov, N. S., Rheological Properties of Coals in the Plastic State, *Solid Fuel Chem.* (Engl. Transl. of Khim. Tverdogo Topl.) **15**(2), 27–32, 1981

12. McDuffie, G. E., and Barr, T., Pressure Viscometer for Viscosities Between 1 to 10^4 P, *Rev. Sci. Instrum.* **40**(5), 653–655, 1969.

13. Claesson, S., All, S., and McAtee, J. L., Jr., New Types of Viscometer Plummets for Measuring Viscosity of Low Viscous

Liquids Under Pressure, *Ind. Eng. Chem., Process Design Develop.* **22**(4), 633–635, 1983.

14. Dandridge, A., and Jackson, D. A., Measurements of Viscosity Under Pressure: A New Method, *J. Phys. D: Appl. Phys.* **14**(5), 829–831, 1981.

15. Jackson, D. A., and Bedborough, D. S., An Application of Intensity Fluctuation Spectroscopy to the Slug Method of Viscosity Determination, *J. Phys. D: Appl. Phys.* **11**, L135–137, 1978.

16. Ramsteiner, F., Falling Cylinder Viscometer for Determination of the Viscosity of Polymer Melts under Hydrostatic Pressure, *Rheol. Acta* **15**(7–8), 427–6433, 1976.

17. Chen, M. C. S., Lescarboura, J. A., and Swift, G. W., The Effect of Eccentricity on the Terminal Velocity of the Cylinder in a Falling Cylinder Viscometer, *AIChE J.* **14**(1), 123–127, 1968.

18. Irving, J. B., The Effect of Non Vertical Alignment on the Performance of a Falling-Cylinder Viscometer, *J. Phys. D: Appl. Phys.* **5**, 214–224, 1972.

19. Wehbeh, E. G., Ui, T. J., and Hussey, R. G., End Effects for the Falling Cylinder Viscometer, *Phys. Fluids A* **5**(1), 25–33, 1993.

20. Chen, M. C. S., and Swift, G. W., Analysis of Entrance and Exit Effects in a Falling Cylinder Viscometer, *AIChE J.* **18**(1), 146–149, 1972.

21. Park, N. A., and Irvine, T. F., Jr., Falling Needle Viscometer. A New Technique for Viscosity Measurements, *Waerme. Stoffuebertrag.* **18**(4), 201–206, 1984.

22. Kim, I., Irvine, T. F., Jr., and Park, N. A., Experimental Study of the Velocity Field Around a Falling Needle Viscometer, *Rev. Sci. Instrum.* **5**(1), 224–228, 1994.

23. Park, N. A., Irvine, T. F., and Gui, F., Yield Stress Measurement with Falling Needle Viscometer, Xth Int. Congress Rheology, Sidney, Australia, 1988.

24. Park, N. A., Irvine,T. F., and Gui, F., Maximum Operating Needle Reynolds Number for the Falling Needle Viscometer, 63rd Annual Meeting Int. Soc. Rheol., New York, 1991.

25. Irvine, T. F., Jr., Park, N., Gui, F., and Park S. S., A High Pressure Falling Needle Viscometer, Presented at Theoretical and Applied Rheology, XIth Int. Cong. Rheol., Brussels, Belgium, August 1992.

26. Park, N. A., and Irvine, T. F., Measurements of Rheological Fluid Properties with the Falling Needle Viscometer, *Rev. Sci. Instrum.* **59**(9), 2051–2058, 1988.

27. Irving, J. B., and Barlow, A. J., An Automatic High Pressure Viscometer, *J. Phys. E: Sci. Instrum.* **4**, 232–236, 1971.

28. Mclachlan, R. J., A New High Pressure Viscometer for Viscosity Range 10 to 10^6 Pa s, *J. Phys. E: Sci. Instrum.* **9**, 391–394, 1976.

29. Patanker, S. V., *Numerical Heat Transfer and Fluid Flow*, Mc-Graw-Hill, New York, 1980.

30. Anderson, D. A., Tannehill, J. C., and Pletcher, R. H., *Computational Fluid Mechanics/Heat Transfer*, McGraw-Hill, New York, 1984.

31. Sutterby, J. L., Falling Sphere Viscometer. 2. End Effects in Short Tubes, *Trans. Soc. Rheol.* **17**(4), 575–585, 1973.

32. Tanner, R. I., End Effects in Falling Ball Viscometry, *J. Fluid Mech.* **17**, 161–170, 1963.